Universal scaling for the spin-electricity conversion on surface states of topological insulators

K. T. Yamamoto,[1] Y. Shiomi,[1,2,*] Kouji Segawa,[3,4] Yoichi Ando,[3,5] and E. Saitoh[1,2,6,7]
[1]*Institute for Materials Research, Tohoku University, Sendai 980-8577, Japan*
[2]*Spin Quantum Rectification Project, ERATO, Japan Science and Technology Agency, Aoba-ku, Sendai 980-8577, Japan*
[3]*Institute of Scientific and Industrial Research, Osaka University, Ibaraki, Osaka 567-0047, Japan*
[4]*Department of Physics, Kyoto Sangyo University, Kyoto 603-8555, Japan*
[5]*Institute of Physics II, University of Cologne, D-50937 Cologne, Germany*
[6]*WPI Advanced Institute for Materials Research, Tohoku University, Sendai 980-8577, Japan*
[7]*Advanced Science Research Center, Japan Atomic Energy Agency, Tokai 319-1195, Japan*
(Received 29 March 2016; revised manuscript received 25 May 2016; published 5 July 2016)

We have investigated spin-electricity conversion on surface states of bulk-insulating topological insulator (TI) materials using a spin-pumping technique. The sample structure is Ni-Fe|Cu|TI trilayers, in which magnetic proximity effects on the TI surfaces are negligibly small owing to the inserted Cu layer. Voltage signals produced by the spin-electricity conversion are clearly observed and are enhanced with decreasing temperature, in line with the dominant surface transport at lower temperatures. The efficiency of the spin-electricity conversion is greater for TI samples with a higher resistivity of bulk states and longer mean free path of surface states, consistent with the surface spin-electricity conversion.

DOI: 10.1103/PhysRevB.94.024404

I. INTRODUCTION

Injection and detection of nonequilibrium spins are key techniques in the field of spintronics [1]. A powerful method to inject spins is spin pumping. Spin pumping enables dynamical spin injection from a ferromagnet into an adjacent nonmagnetic metal, which is induced by coherent precession of magnetization at ferromagnetic resonance (FMR) [2]. In spin-pumping experiments, bilayers comprising ferromagnetic $Ni_{81}Fe_{19}$ (permalloy, Py) and nonmagnetic Pt have been studied as a typical system [2–6]. Although Pt has been widely used for spin detection owing to its strong spin-orbit interaction, the search for more efficient spin detectors is one of the urgent issues in the spintronics field [7,8].

A topological insulator (TI) is a promising material for spintronics application because of its potential for highly efficient spin-electricity conversion [9,10]. Topological insulators are a state of quantum matter [11–13] in which the surface is metallic while the interior is insulating. Spin-electricity conversion on TI materials has recently been investigated using spin pumping for bulk-metallic samples (Bi_2Se_3) [14–16] and also for bulk-insulating ones [17]. In a previous report [17], some authors of the present paper demonstrated the spin-electricity conversion induced by spin pumping into surface states of TIs, $Bi_{1.5}Sb_{0.5}Te_{1.7}Se_{1.3}$ (BSTS) [18,19] and Sn-doped Bi_2Te_2Se (SnBTS) [20] in contact with Py. Since millimeter-thick TI samples were used in [17], the inverse spin Hall signal from bulk carriers is neglected (see Appendix A), and the observed spin-electricity conversion signal is safely ascribed to a surface contribution. The sign of the generated electric signals is consistent with the spin-electricity conversion on the topological surface state [17], whereas the opposite sign is expected for coexisting Rashba surface states [21–24]. On the surface states of TIs, since spin direction and electron-flow direction have one-to-one correspondence (the spin-momentum locking), injected spins are converted into electric currents along an in-plane direction on the surface when the bulk state is sufficiently insulating. Although highly efficient spin-electricity conversion has been reported for bulk-metallic TIs [9,10,16], the reported value for bulk-insulating BSTS is ∼0.01% [17,25].

Although the spin-electricity conversion on the topological surface states was demonstrated using a spin-pumping technique [17], it remains unclear how the produced electric signal is related to the surface transport properties of TI materials. In this paper, we study spin-electricity conversion induced by spin pumping for several SnBTS samples whose bulk-insulating properties are ideal for its detailed study. By inserting a thin Cu layer between Py and TI layers, magnetic proximity effects to TI surfaces are negligible. The efficiency of the observed spin-electricity conversion is found to be greater for TI materials with higher bulk resistivity and longer surface mean path. This result shows that the spin-electricity conversion takes places at the surface state and also that its efficiency strongly depends on surface transport properties.

II. EXPERIMENTAL DETAILS

We used SnBTS to investigate the spin-electricity conversion effect on topological surface states. The single crystals of 0.5% Sn-doped Bi_2Te_2Se were synthesized using the Bridgman method [20]. Since the bulk state of SnBTS is more insulating than that of BSTS [20,26], SnBTS has been considered as an ideal system for transport study of Dirac surface states [26]. Three SnBTS samples (SnBTS1, whose size is 3.3 × 1.2 × 0.4 mm; SnBTS2, 3.3 × 2.2 × 0.3 mm; and SnBTS3, 3.0 × 1.5 × 0.7 mm) were used in this study. These samples were cut from one boule of SnBTS crystals.

The experimental setup of the spin-pumping measurement is almost the same as that in our previous report [17]. Schematic illustrations of the sample and experimental setup are shown in Figs. 1(a) and 1(b). A 5-nm-thick Cu film and 25-nm-thick Py film were evaporated on the middle part of a cleaved

*Corresponding author: shiomi@imr.tohoku.ac.jp

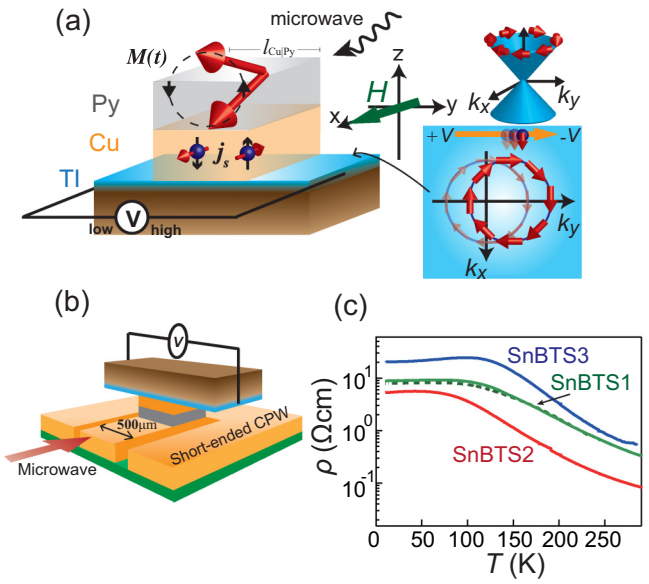

FIG. 1. (a) Experimental setup of spin-electricity conversion induced by spin pumping into topological insulators (TIs). "High" and "low" indicate input codes of the nanovoltmeter (Keithley 2182A). On the topological surface state, spin polarization produces spin-electricity conversion voltage in the Hall direction. The origin of this electric signal is a shift of the surface Fermi surface induced by spin injection. (b) A schematic illustration of the sample setting and the coplanar waveguide. (c) Temperature T dependence of the in-plane resistivity ρ for three Sn-doped Bi_2Te_2Se samples (SnBTS1, SnBTS2, and SnBTS3). For SnBTS1, after the spin-pumping measurement, the Py|Cu layer was removed, and then the resistivity was measured again (dashed curve). The bulk-insulating property is not changed by the deposition of metallic films or the measurement of spin pumping.

surface of TI samples in a high vacuum. The roughness of TI surfaces measured by atomic force microscopy is about 1 nm (see Appendix B). The length of Cu and Py films $l_{Cu|Py}$ is 0.5 mm. In the spin-pumping measurement, magnetization dynamics in Py was excited by a microwave magnetic field on a coplanar-type waveguide in an in-plane static magnetic field H [Fig. 1(b)]. We used a commercial network analyzer as a microwave source. Microwave frequency was kept at 5 GHz, and the power of the incident microwave was amplified 1000 times by a commercial microwave amplifier. While sweeping the external magnetic field, the FMR spectrum in Py and electromotive force arising between the ends of TI samples were recorded simultaneously using the network analyzer and a nanovoltmeter, respectively. The measurements were conducted at low temperatures down to 10 K in a probe station.

III. RESULTS AND DISCUSSION

Figure 1(c) shows the temperature T dependence of resistivity ρ for the TI samples. ρ at room temperature is 0.05–1 Ω cm and increases with decreasing T, which indicates that the bulk carriers are compensated in all the TI samples. Using the activation law above 200 K, values of the energy gap are estimated to be 80–100 meV, similar to a reported value (65 meV) [20]. At low temperatures below ∼100 K, the resistivity begins to decrease, which is unusual for traditional semiconductors. Metallic surface conduction is dominant in the low-T region. It is noted that the temperature dependence of ρ for SnBTS1 hardly changed after the measurement of spin pumping (Fig. 2), as shown by the dotted curve in Fig. 1(c). The sample qualities were not degraded by the deposition of Py|Cu bilayers or the spin-pumping measurement.

We performed spin-pumping experiments for the TI samples attached with Cu and Py films. Figure 2(a) shows the magnetic field H dependence of microwave transmittance $|S_{21}|^2$ for Py|Cu|SnBTS1 at several temperatures. Clear dips which correspond to FMR in Py were observed at each temperature around ±30 mT. The FMR field is almost constant with temperature, which shows that the magnetic properties of the Py layer hardly change with temperature. The magnitude of resonance absorption slightly decreases with decreasing T because of an increase in the microwave loss in our microwave circuit.

Figure 2(b) shows the magnetic field H dependence of voltage signals arising at FMR magnetic fields for Py|Cu|SnBTS1 at various temperatures. At any temperature, the voltage peaks are clearly observed at FMR magnetic fields $\pm H_{FMR}$ of Py. The sign of the voltage peaks is negative at both $+H_{FMR}$ and $-H_{FMR}$ above 100 K. The magnitudes of the voltage peaks at $\pm H_{FMR}$ are almost the same at 280 K, while they are clearly different at 120 K. At high temperatures, the Seebeck effect of bulk carriers independent of magnetic fields dominates the peak signals [17]. An origin of this Seebeck voltage is a small in-plane temperature gradient (∼50 mK/mm [17]) due to the inevitable heating effects at FMR [17]. The Seebeck effect resulting from asymmetry in the sample shape and wiring is significant at high temperatures because this system is well known to be a good thermoelectric material. As temperature decreases, the magnitude of the Seebeck voltage decreases since the excitation of bulk carriers is suppressed at lower temperatures. Below 80 K, the sign reversal between $+H_{FMR}$ and $-H_{FMR}$ is observed, as shown in Fig. 2(b), indicating that the spin-electricity conversion signal is dominant. The peak sign at $+H_{FMR}$ is negative, consistent with that reported in [17].

The magnitude of the spin-electricity conversion voltage increases with decreasing temperature, consistent with the dominant surface conduction at lower temperatures. Figure 2(c) shows the H dependence of the antisymmetric part of the voltage peak $|V^a| \equiv |V(H) - V(-H)|/2$ divided by resonance absorption power ΔP for Py|Cu|SnBTS1. Here, ΔP is calculated from the microwave transmittance data for the same sample as in Fig. 2(a) [17]. As shown in Fig. 2(c), the magnitude of $|V^a/\Delta P|$ monotonically increases with decreasing T from 220 to 40 K for Py|Cu|SnBTS1.

Figure 3 summarizes the T dependence of the antisymmetric signals for all the samples. Here, the antisymmetric signal $|V^a/\Delta P|$ is normalized by the sample size; the produced electric field $E^a \equiv V^a/l_{Cu|Py}$ divided by the resonance absorption power per unit area $\Delta\tilde{P}$ is plotted in Fig. 3. As shown in Fig. 3, $|E^a/\Delta\tilde{P}|$ for the three samples is small and almost constant above 200 K. The magnitudes of $|E^a/\Delta\tilde{P}|$ are similar for all the samples in the high-T range. This small constant signal at high temperatures may result from ferromagnetic transports in the Py layer; small and constant

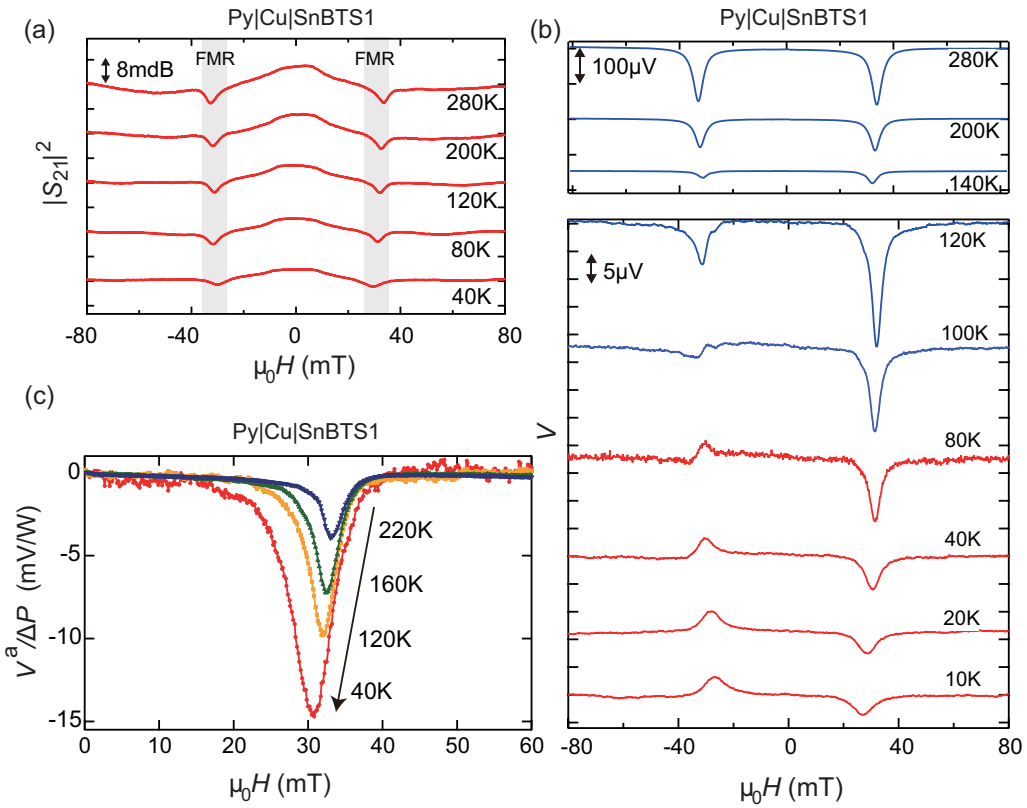

FIG. 2. (a) Magnetic field H dependence of microwave transmittance $|S_{21}|^2$ for Py|Cu|SnBTS1 at some temperatures. The data are shifted vertically just for clarity. (b) Magnetic field H dependence of the voltage signal V arising around FMR magnetic fields of Py for Py|Cu|SnBTS1 at various temperatures. The data are shifted vertically just for clarity. (c) H dependence of the antisymmetric part of V (V^a) normalized by the resonance absorption power ΔP for Py|Cu|SnBTS1 at several temperatures.

voltage signals are similarly observed in Py|Cu|SiO_2, as shown in Fig. 3 [17]. In the high-temperature range where the bulk conduction is dominant, the injected spin current and also the converted electric current are totally shunted in the conductive bulk state of our thick TI samples. With decreasing temperature

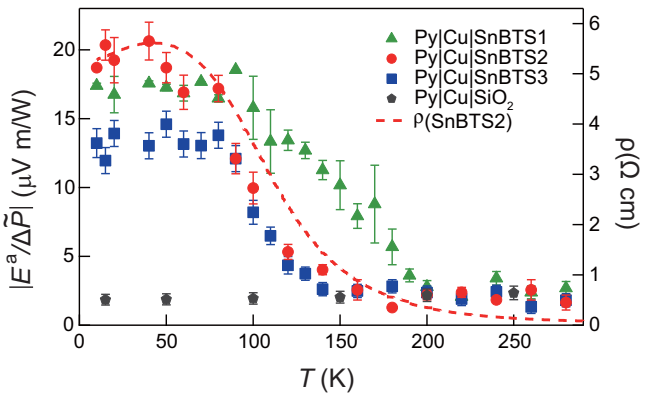

FIG. 3. Temperature T dependence of the antisymmetric part of the electric field E^a ($= V^a/l_{\mathrm{Cu|Py}}$), divided by the resonance absorption power per unit area $\Delta\tilde{P}$ for the Py|Cu|SnBTS samples. The absolute values of $E^a/\Delta\tilde{P}$ are plotted. For comparison, $|E^a/\Delta\tilde{P}|$ for a Py|Cu film grown simultaneously on an insulating thermally oxidized Si substrate is plotted. The T dependence of resistivity ρ for SnBTS2 is also shown for comparison (dashed curve).

below 150–200 K, $|E^a/\Delta\tilde{P}|$ begins to increase rapidly for the Py|Cu|SnBTS samples. This sharp enhancement of $|E^a/\Delta\tilde{P}|$ at low temperatures is clearly correlated with the resistivity increase at low temperatures, as shown by the dotted curve in Fig. 3. As the bulk resistivity increases at lower temperatures, the spin polarization accumulated near the TI surface increases, and greater spin-electricity conversion signals may appear. The magnitude of $|E^a/\Delta\tilde{P}|$ at the lowest temperature is similar for all the samples, whereas the resistivity values are rather different among them [Fig. 1(c)].

We analyze the efficiency of the spin-electricity conversion in terms of the mean free path on the surface λ for each sample. The inverse Edelstein effect length $\lambda_{\mathrm{IEE}} \equiv j_c^{2D(y)}/j_{s(x)}^{3D}$ [27–29] for the Py|Cu|SnBTS samples and also for Py|Bi_2Se_3 (Py|BS) and Py|$Bi_{1.5}Sb_{0.5}Te_{1.7}Se_{1.3}$3 (Py|BSTS3) reported in [17] (see also [30]) is calculated by dividing the surface electric current density $j_c^{2D(y)}$ by the spin current density $j_{s(x)}^{3D}$ [5]. Here, $j_c^{2D(y)}$ is calculated by $\{E^a(10\,\mathrm{K}) - E^a(293\,\mathrm{K})\}/R_t$, where R_t is the total sheet resistance for the Py|Cu layer and the TI layer in parallel. To estimate the charge current originating from the spin-electricity conversion $j_c^{2D(y)}$, we subtract the electric current originating from the ferromagnetic transports in the Py layer, $E^a(293\mathrm{K})/R_t$; as shown in Fig. 3, the generated electric field is small and constant above 200 K because shunting effects strongly suppress the spin-electricity conversion signal in the high-T range. For $j_{s(x)}^{3D}$, we used the following expression

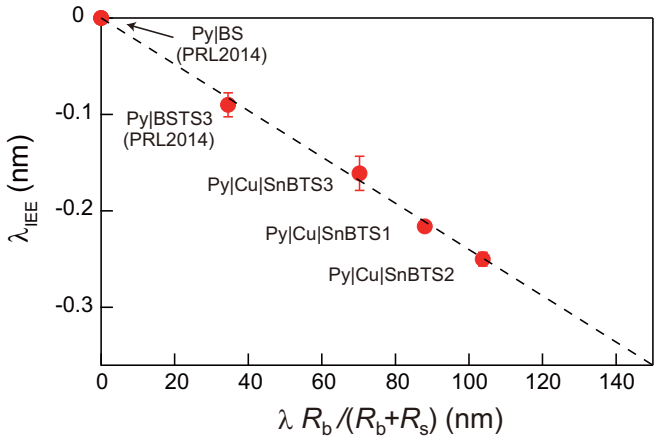

FIG. 4. The inverse Edelstein effect length λ_{IEE} ($= j_c^{2D(y)}/j_{s(x)}^{3D}$) as a function of $\lambda R_s/(R_s + R_b)$ for various samples. $j_c^{2D(y)}$ and $j_{s(x)}^{3D}$ indicate the electric current density generated on the TI surface and the spin current density injected from Py, respectively. Here, e, λ, R_s, and R_b denote the elementary charge, the mean free path on the surface, and the sheet resistances for the surface and bulk parts, respectively. The voltage-peak magnitude at the lowest temperature was used to calculate $j_c^{2D(y)}$. The experimental results for Py|BS and Py|BSTS3 reported in [17] are also plotted.

established for spin pumping [5,31]:

$$j_{s(x)}^{3D} = \frac{4e}{g\mu_B}\frac{\mu_0\Delta H_{\mathrm{Py|Cu|TI}} - \mu_0\Delta H_{\mathrm{Py|Cu}}}{\mu_0\Delta H_{\mathrm{Py|Cu|TI}}} \times \frac{1}{\sqrt{M^2 + (2\omega/\gamma)^2}}\Delta\tilde{P}. \quad (1)$$

Here, e is the elementary charge ($e = 1.602 \times 10^{-19}$ C), g is the g factor ($g = 2.12$), μ_B is the Bohr magneton ($\mu_B = 9.27 \times 10^{-24}$ J/T), $(\mu_0\Delta H_{\mathrm{Py|Cu|TI}} - \mu_0\Delta H_{\mathrm{Py|Cu}})/\mu_0\Delta H_{\mathrm{Py|Cu|TI}}$ is the change in the linewidth of FMR in the presence of the TI layer [$(\mu_0\Delta H_{\mathrm{Py|Cu|TI}} - \mu_0\Delta H_{\mathrm{Py|Cu}})/\mu_0\Delta H_{\mathrm{Py|Cu|TI}} = 0.120$ for Py|Cu|SnBTS samples; see Appendix C], M is the magnetization of Py ($M = 0.80$ T), ω is the angular frequency of the microwave ($\omega = 3.14 \times 10^{10}$ s^{-1}), and γ is the gyromagnetic ratio ($\gamma = 1.76 \times 10^{11}$ s^{-1} T^{-1}). The obtained magnitudes of $j_{s(x)}^{3D}$ are 1.93×10^6 A/m^2 for Py|Cu|SnBTS1, 1.98×10^6 A/m^2 for Py|Cu|SnBTS2, and 1.90×10^6 A/m^2 for Py|Cu|SnBTS3 at the incident microwave power of 0.316 mW.

The obtained λ_{IEE} is plotted against $\lambda R_b/(R_b + R_s)$ for each sample in Fig. 4. Here, R_s and R_b are the surface and bulk sheet resistances for TI samples, respectively. R_b and R_s are separated from each other by fits to the ρ-T curve [Fig. 1(c)] using the three-dimensional variable-range hopping formula ($\sim T^{-1/4}$) in a low-T range [19]. λ is estimated from the reported Fermi wave number k_F (5.9×10^{-2} Å^{-1} for SnBTS [20,26] and 1.0×10^{-1} Å^{-1} for BSTS [32]) and from R_s estimated for each sample using the relation $\lambda = h/(2e^2 R_s k_F)$ [33–35]. Here, it is noted that the Fermi wave number k_F was reported for the same SnBTS [20] and BSTS [32] samples as those used in this paper, which were grown by some of the present authors in the same conditions using the same instruments. For the bulk-metallic TI samples (BS) with ∼0.1 mm thickness, R_b is as small as ∼1 mΩ [17], which is much smaller than the surface sheet resistance R_s [36]. Hence, $R_b/(R_b + R_s) \approx 0$, and the spin-electricity conversion signal is not observed [17] (Fig. 4). For the bulk-insulating TI samples, by contrast, both $j_c^{2D(y)}$ and $R_b/(R_b + R_s)$ exhibit sizable values. As shown in Fig. 4, a clear linear relation is observed, which shows that the spin-electricity conversion efficiency is greater for TI samples with higher bulk resistivity and longer surface mean free path. Experimental results for Py|BSTS1 and Py|BSTS2 in the literature [17] are not shown in Fig. 4 since the antisymmetric parts of the voltage peaks are not discerned above 100 K due to very large Seebeck voltages [17].

The linear dependence of the inverse Edelstein effect length on the mean free path on the surface is consistent with the theoretical prediction [27–29]. The relation between the generated electric current and the spin polarization $\langle\sigma_x\rangle$ is given by $j_c^{2D(y)} \approx (-2e/\hbar)v_F\langle\sigma_x\rangle$ [37], where v_F is the Fermi velocity for the surface state. The spin polarization on the surface is produced by injection of the spin current $j_{s(x)}^{3D}$ from Py, following $\langle\sigma_x\rangle/\tau = (\hbar/2e)j_{s(x)}^{3D}R_b/(R_b + R_s)$ (with τ being the scattering relaxation time for the surface) [17]. Hence, we obtain $j_c^{2D(y)}/j_{s(x)}^{3D} \approx -\lambda R_b/(R_b + R_s)$. This relation well explains the experimental results in Fig. 4. It is interestingly noted that the slope of the linear fit in Fig. 4 corresponds to the spin injection efficiency η [17]. The obtained value is $\eta \approx 2.4 \times 10^{-3}$ (0.24%), which is comparable to the values reported for bulk-insulating BSTS samples [17,25]. Since the spin injection efficiency indicates the ratio of the spin polarization on the TI surface to the injected spin angular momentum from Py, the low value of η does not mean that the "spin Hall angle" for the topological surface state is very small. The low η value might be related to the adsorbents on the TI surface (Appendix B) caused by the short-time air exposure before the metal deposition and the resulting poor-quality interface.

IV. SUMMARY

In summary, we measured spin-electricity conversion induced by spin pumping into Sn-doped Bi_2Te_2Se at low temperatures. To prevent magnetic proximity effects from ferromagnetic layers, a thin Cu layer was inserted between Py and TI. At FMR in Py, the spin-electricity conversion voltage was observed and enhanced with decreasing temperature. The spin-electricity conversion efficiency at low temperatures is found to increase with increasing magnitudes of bulk resistivity and surface mean free path, following a single scaling law. This result is consistent with theories on spin-electricity conversion on the topological surface state.

ACKNOWLEDGMENTS

We thank M. Novak and Z. Wang for their help in crystal growth. K.T.Y. acknowledges the support from the Leading Graduates Schools Program (Tohoku University "MD program") by MEXT. Y.S. would like to acknowledge the support from the Motizuki Fund of Yukawa Memorial

Foundation. This work was supported by JSPS (KAKENHI No. 25220708 and No. 16H00977 and the Core-to-Core program "International research center for new-concept spintronics devices") and MEXT [Innovative Area "Nano Spin Conversion Science" (No. 26103005)].

K.T.Y. and Y.S. contributed equally to this work.

APPENDIX A: SIMULATION OF INVERSE SPIN HALL VOLTAGE FOR THE BULK STATE OF A TI SAMPLE

To present more clearly the concept that bulk-form TI materials are useful for the study of the surface spin-electricity conversion, the magnitude of the inverse spin Hall voltage for bulk carriers of Bi_2Se_3 is simulated as a function of the TI thickness t_{TI} in Fig. 5. Here, the surface spin-electricity conversion (inverse Edelstein effect) is neglected, and only the bulk inverse spin Hall effect is considered. For calculation of the inverse spin Hall voltage, Eq. (22) in [5] was used. For simulation parameters, the spin-diffusion length is 6.2 nm [15], the spin Hall angle is 0.0093 [15], and the sheet resistance for the Py layer is 16 Ω. It is noted that for Py|Pt [38] and YIG|Pt [39] systems, a similar Pt thickness dependence of the inverse spin Hall voltage was already verified experimentally.

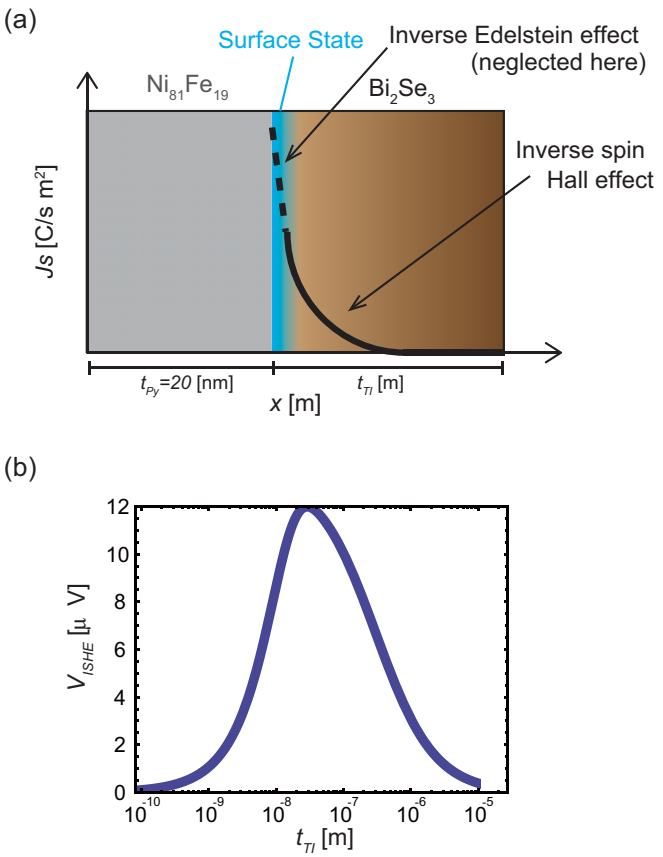

FIG. 5. (a) Setup of a simulation of the inverse spin Hall voltage expected for the bulk state of TI. As the TI material, Bi_2Se_3 is selected. Here, the surface spin-electricity conversion is neglected, and only the inverse spin Hall effect for bulk-state carriers is considered. t_{TI} is the thickness of the TI layer. (b) A simulation result for the magnitude of the inverse spin Hall voltage as a function of t_{TI}. The relation used for this simulation is Eq. (22) in [5]. For simulation parameters, the spin-diffusion length is 6.2 nm [15], the spin Hall angle is 0.0093 [15], and the sheet resistance for the Py layer is 16 Ω.

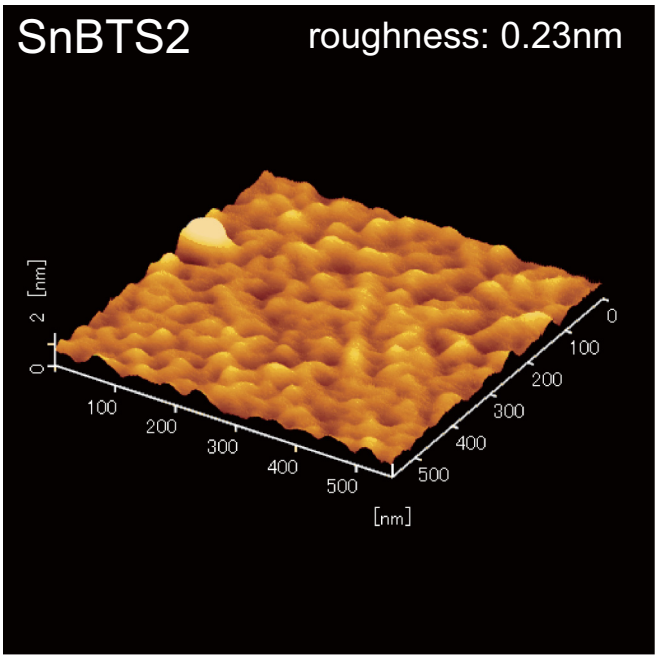

FIG. 6. Surface roughness for SnBTS2. The average roughness is 0.23 nm.

APPENDIX B: EVALUATION OF SURFACE MORPHOLOGY BY ATOMIC FORCE MICROSCOPY

The surface morphology evaluated by atomic force microscopy for SnBTS2 is shown in Fig. 6. The averaged roughness is 0.23 nm, which is less than the height of one quintuple layer and hence is most likely due to adsorbed molecules. All the TI samples that we used have similar values of surface roughness.

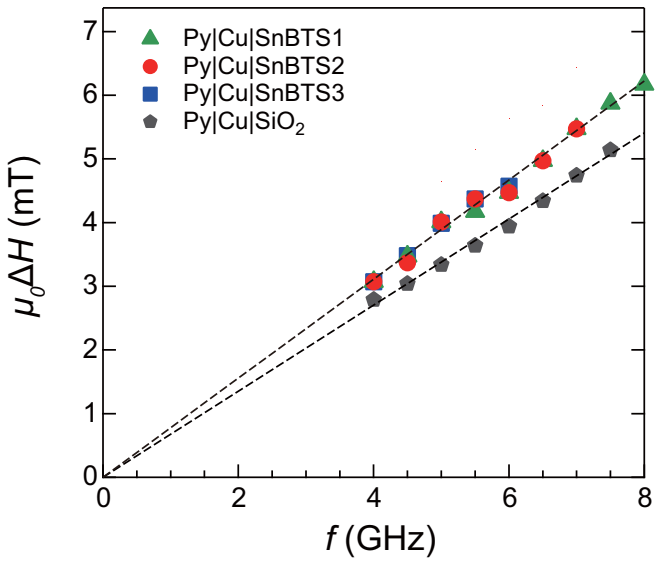

FIG. 7. Microwave frequency dependence of the intrinsic FMR linewidth ΔH for Py|Cu|SnBTS samples and Py|Cu|SiO_2.

APPENDIX C: FREQUENCY DEPENDENCE OF THE FMR LINEWIDTH

The frequency dependence of the intrinsic FMR linewidth ΔH for the Py layer is shown in Fig. 7. ΔH is obtained from the fits to FMR spectra using a Lorentzian function [17].

[1] S. Maekawa, S. O. Valenzuela, E. Saitoh, and T. Kimura, *Spin Current* (Oxford University Press, Oxford, 2012).

[2] E. Saitoh, M. Ueda, H. Miyajima, and G. Tatara, Appl. Phys. Lett. **88**, 182509 (2006).

[3] A. Azevedo, L. H. V. Leao, R. L. Rodriguez-Suarez, A. B. Oliveira, and S. M. Rezende, J. Appl. Phys. **97**, 10C715 (2005).

[4] M. V. Costache, M. Sladkov, S. M. Watts, C. H. van der Wal, and B. J. van Wees, Phys. Rev. Lett. **97**, 216603 (2006).

[5] K. Ando, S. Takahashi, J. Ieda, Y. Kajiwara, H. Nakayama, T. Yoshino, K. Harii, Y. Fujikawa, M. Matsuo, S. Maekawa, and E. Saitoh, J. Appl. Phys. **109**, 103913 (2011).

[6] O. Mosendz, J. E. Pearson, F. Y. Fradin, G. E. W. Bauer, S. D. Bader, and A. Hoffmann, Phys. Rev. Lett. **104**, 046601 (2010).

[7] Y. Niimi, Y. Kawanishi, D. H. Wei, C. Deranlot, H. X. Yang, M. Chshiev, T. Valet, A. Fert, and Y. Otani, Phys. Rev. Lett. **109**, 156602 (2012).

[8] K. Fujiwara, Y. Fukuma, J. Matsuno, H. Idzuchi, Y. Niimi, Y. Otani, and H. Takagi, Nat. Commun. **4**, 2893 (2013).

[9] A. R. Mellnik, J. S. Lee, A. Richardella, J. L. Grab, P. J. Mintun, M. H. Fischer, A. Vaezi, A. Manchon, E.-A. Kim, N. Samarth, and D. C. Ralph, Nature (London) **511**, 449 (2014).

[10] Y. Fan, P. Upadhyaya, X. Kou, M. Lang, S. Takei, Z. Wang, J. Tang, L. He, L.-T. Chang, M. Montazeri, G. Yu, W. Jiang, T. Nie, R. N. Schwartz, Y. Tserkovnyak, and K. L. Wang, Nat. Mater. **13**, 699 (2014).

[11] Y. Ando, J. Phys. Soc. Jpn. **82**, 102001 (2013).

[12] M. Z. Hasan and C. L. Kane, Rev. Mod. Phys. **82**, 3045 (2010).

[13] X.-L. Qi and S.-C. Zhang, Rev. Mod. Phys. **83**, 1057 (2011).

[14] A. A. Baker, A. I. Figueroa, L. J. Collins-McIntyre, G. van der Laan, and T. Hesjedal, Sci. Rep. **5**, 7907 (2015).

[15] P. Deorani, J. Son, K. Banerjee, N. Koirala, M. Brahlek, S. Oh, and H. Yang, Phys. Rev. B **90**, 094403 (2014).

[16] M. Jamali, J. S. Lee, J. S. Jeong, F. Mahfouzi, Y. Lv, Z. Zhao, B. K. Nikolic, K. A. Mkhoyan, N. Samarth, and J.-P. Wang, Nano Lett. **15**, 7126 (2015).

[17] Y. Shiomi, K. Nomura, Y. Kajiwara, K. Eto, M. Novak, K. Segawa, Y. Ando, and E. Saitoh, Phys. Rev. Lett. **113**, 196601 (2014).

[18] A. A. Taskin, Z. Ren, S. Sasaki, K. Segawa, and Y. Ando, Phys. Rev. Lett. **107**, 016801 (2011).

[19] Z. Ren, A. A. Taskin, S. Sasaki, K. Segawa, and Y. Ando, Phys. Rev. B **84**, 165311 (2011).

[20] Z. Ren, A. A. Taskin, S. Sasaki, K. Segawa, and Y. Ando, Phys. Rev. B **85**, 155301 (2012).

[21] P. D. C. King *et al.*, Phys. Rev. Lett. **107**, 096802 (2011).

[22] M. S. Bahramy, P. D. C. King, A. de la Torre, J. Chang, M. Shi, L. Patthey, G. Balakrishnan, Ph. Hofmann, R. Arita, N. Nagaosa, and F. Baumberger, Nat. Commun. **3**, 1159 (2012).

[23] S. Hong, V. Diep, S. Datta, and Y. P. Chen, Phys. Rev. B **86**, 085131 (2012).

[24] F. Yang, S. Ghatak, A. A. Taskin, K. Segawa, Y. Ando, M. Shiraishi, Y. Kanai, K. Matsumoto, A. Rosch, and Y. Ando, arXiv:1605.04149.

[25] Y. Ando, T. Hamasaki, T. Kurokawa, K. Ichiba, F. Yang, M. Novak, S. Sasaki, K. Segawa, Y. Ando, and M. Shiraishi, Nano Lett. **14**, 6226 (2014).

[26] S. K. Kushwaha, Q. D. Gibson, J. Xiong, I. Pletikosic, A. P. Weber, A. V. Fedorov, N. P. Ong, T. Valla, and R. J. Cava, J. Appl. Phys. **115**, 143708 (2014).

[27] J. C. Rojas-Sánchez *et al.*, Nat. Commun. **4**, 2944 (2013).

[28] J. C. Rojas-Sánchez, S. Oyarzun, Y. Fu, A. Marty, C. Vergnaud, S. Gambarelli, L. Vila, M. Jamet, Y. Ohtsubo, A. Taleb-Ibrahimi, P. Le Fevre, F. Bertran, N. Reyren, J.-M. George, and A. Fert, Phys. Rev. Lett. **116**, 096602 (2016).

[29] K. Shen, G. Vignale, and R. Raimondi, Phys. Rev. Lett. **112**, 096601 (2014).

[30] The experimental results in [17] are reanalyzed for the plot in Fig. 4. For Py|BSTS3, the temperature dependence of $V^a/\Delta P$ is shown in Fig. S11 in the Supplemental Material of [17].

[31] S. Mizukami, Y. Ando, and T. Miyazaki, Phys. Rev. B **66**, 104413 (2002).

[32] T. Arakane, T. Sato, S. Souma, K. Kosaka, K. Nakayama, M. Komatsu, T. Takahashi, Z. Ren, K. Segawa, and Y. Ando, Nat. Commun. **3**, 636 (2011).

[33] D. Culcer, Physica E (Amsterdam, Neth.) **44**, 860 (2012).

[34] S. Das Sarma, S. Adam, E. H. Hwang, and E. Rossi, Rev. Mod. Phys. **83**, 407 (2011).

[35] This relation (p. 442 in [34]) is obtained from the Boltzmann transport theory for two-dimensional electron systems. The estimated values are $\lambda = 8.8 \times 10^1$ nm for Py|Cu|SnBTS1, $\lambda = 1.04 \times 10^2$ nm for Py|Cu|SnBTS2, $\lambda = 7.0 \times 10^1$ nm for Py|Cu|SnBTS3, and $\lambda = 2.1 \times 10^1$ nm for Py|BSTS3 in [17]. Note that the λ values reported for SnBTS and BSTS samples in measurements of the Shubnikov–de Haas effect [18–20] are 20–50 nm, which are almost similar to the λ values estimated by the above simple formula.

[36] A. A. Taskin, S. Sasaki, K. Segawa, and Y. Ando, Phys. Rev. Lett. **109**, 066803 (2012).

[37] A. A. Burkov and D. G. Hawthorn, Phys. Rev. Lett. **105**, 066802 (2010).

[38] H. Nakayama, K. Ando, K. Harii, T. Yoshino, R. Takahashi, Y. Kajiwara, K. Uchida, Y. Fujikawa, and E. Saitoh, Phys. Rev. B **85**, 144408 (2012).

[39] V. Castel, N. Vlietstra, J. Ben Youssef, and B. J. van Wees, Appl. Phys. Lett. **101**, 132414 (2012).